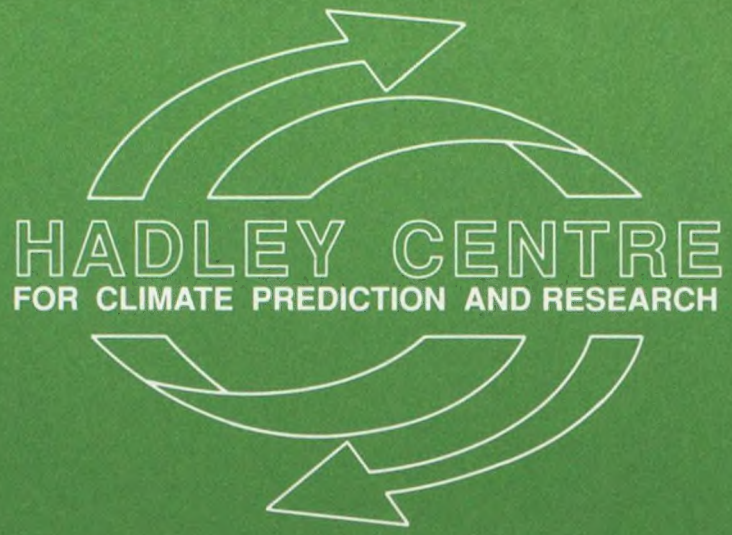

Seasonal variations of the clear-sky greenhouse effect: the role of changes in atmospheric temperatures and humidities

by

M.J.Webb, A.Slingo and G.L.Stephens

CRTN 41 September 1993

CLIMATE
RESEARCH
TECHNICAL
NOTE

Hadley Centre
Meteorological Office
London Road
Bracknell
Berkshire RG12 2SY

CLIMATE RESEARCH TECHNICAL NOTE NO.41

SEASONAL VARIATIONS OF THE CLEAR-SKY GREENHOUSE EFFECT: THE ROLE OF CHANGES IN ATMOSPHERIC TEMPERATURES AND HUMIDITIES

by

M J Webb, A Slingo and G L Stephens

Submitted to 'Climate Dynamics', April 1993.
Revised version accepted August 1993.

Hadley Centre for Climate Prediction and Research
Meteorological Office
London Road
Bracknell
Berkshire RG12 2SY

NOTE: This paper has not been published. Permission to quote from it should be obtained from the Director of the Hadley Centre.

Seasonal variations of the clear-sky greenhouse effect: the role of changes in atmospheric temperatures and humidities

M. J. Webb[1], A. Slingo[1] and G. L. Stephens[2]

[1] Hadley Centre for Climate Prediction and Research, Meteorological Office, Bracknell, Berkshire, RG12 2SY, UK

[2] Department of Atmospheric Science, Colorado State University, Fort Collins, CO 80523, USA

Submitted to *Climate Dynamics*, April 1993. Revised version accepted August 1993.

Abstract. We present an analysis of the factors which control the seasonal variations of the clear-sky greenhouse effect, based on satellite observations and radiative transfer simulations. The satellite observations include the radiation budget at the top of the atmosphere from the Earth Radiation Budget Experiment and the total column moisture content derived from the Special Sensor Microwave/Imager. The simulations were performed with the SAMSON system, described in an earlier paper, using atmospheric temperatures and humidities from operational analyses produced by the European Centre for Medium Range Weather Forecasts.

At low latitudes, the magnitude of the clear-sky greenhouse effect is dominated by the strong thermodynamic link between the total column moisture content of the atmosphere and sea surface temperatures, with minimal seasonal variations. In contrast, at middle to high latitudes there are strong seasonal variations, the clear-sky greenhouse effect being largest in

Address for correspondence and proofs:
A. Slingo, Hadley Centre for Climate Prediction and Research, Meteorological Office, Bracknell, Berkshire, RG12 2SY, U.K.

winter and smallest in summer. These variations cannot be explained by the seasonal cycle in the total column moisture content, as this is largest in summer and smallest in winter. The variations are controlled instead by the seasonal changes in atmospheric temperatures. The colder atmosphere in winter enhances the temperature differential between the atmosphere and the sea surface, leading to a larger greenhouse effect despite the lower moisture contents. The magnitude of the clear-sky greenhouse effect is thus controlled by atmospheric humidity at low latitudes, but by atmospheric temperature at middle and high latitudes. These controls are illustrated by results from sensitivity experiments with SAMSON and are interpreted in terms of a simple model.

Introduction

Satellite observations have provided valuable insights into the factors which control the greenhouse effect. Spaceborne measurements by the Earth Radiation Budget Experiment (ERBE) of the radiation budget under both clear-sky and cloudy conditions have enabled the effects of clouds to be separated from those of atmospheric gases (Harrison et al. 1990). The cloud studies performed with these data are in part motivated by the need to understand cloud feedbacks, which remain a major source of uncertainty in projections of global climate change (Senior and Mitchell 1993). Despite this, the magnitude of the greenhouse effect at the present time is dominated by the absorption and emission by atmospheric gases, in particular water vapour, rather than by clouds (see next section). In order to understand the greenhouse effect and its relationship to the present climate system, it is therefore essential that the contribution from clear-skies is studied in sufficient detail.

Analyses of the clear-sky greenhouse effect have shown that it is determined primarily by the distributions of temperature and of atmospheric water vapour. Raval and Ramanathan

(1989) used ERBE radiation budget data to demonstrate the existence of a strong positive correlation between the clear-sky greenhouse effect over the oceans and the sea surface temperature (SST). They showed that this was mainly due to the correlation between the total column moisture content w (often referred to as the precipitable water content), derived from satellite passive microwave measurements, and the SST. They argued that these correlations provide observational evidence for a positive water vapour feedback, as predicted by simulations with climate models. Stephens and Greenwald (1991) performed a similar analysis with a more comprehensive dataset and demonstrated that the observed relationships were consistent with a simple grey body radiative model. In addition, they performed numerical experiments which showed that the clear-sky greenhouse effect was not only dependent on w, but also sensitive to the temperature and humidity profiles. Ramanathan and Collins (1991) drew attention to the rapid increase in the magnitude of the clear-sky greenhouse effect as the SSTs reach their maximum values. They referred to this phenomenon as the 'super greenhouse effect' and hypothesized that the enhanced longwave heating is balanced by the shortwave effects of the extensive upper-level stratiform cloud layers which are produced by deep convection. These clouds shade the ocean surface and so might act as a thermostat to keep the SSTs within the observed range. Finally, Duvel and Bréon (1991) used more recent satellite microwave data from the Special Sensor Microwave/ Imager (SSM/I) and examined the change in the clear-sky greenhouse effect associated with interannual changes in SST.

None of these studies examined the seasonal changes in the clear-sky greenhouse effect. These are particularly large at high latitudes, where they produce a significant modulation of the simple dependence on w which is found at low latitudes. This paper analyses these changes and offers a simple explanation in terms of the associated seasonal variations in the atmospheric temperatures and humidities. The approach is to employ the simulation system known as SAMSON (Slingo and Webb 1992) to simulate the seasonal changes and to perform

sensitivity experiments which separate the individual effects of the temperature and humidity variations.

The following section defines the normalised greenhouse effect employed in this study and introduces a simple analytic model which helps to explain the results. Brief details are then given of the SAMSON simulations and of the ERBE and SSM/I data which provide the necessary validation. The SAMSON simulations of the clear-sky emission from the top of the atmosphere are then compared with ERBE. The seasonal changes in the clear-sky greenhouse effect are derived both from the ERBE and SSM/I data and from SAMSON. Finally, SAMSON is used to perform the sensitivity experiments which explain these changes.

The normalized greenhouse effect and a simple model

The greenhouse effect may be defined as the difference between the longwave emission from the surface (E) and the emission from the top of the atmosphere (F):

$$G = E - F \tag{1}$$

In round figures, the global/annual average value of E is 390 Wm^{-2} and that of F is 235 Wm^{-2} (Harrison et al. 1990), so that G is 155 Wm^{-2}.

The clear-sky greenhouse effect G_A may then be defined by substituting the clear-sky value of F into Eq. (1):

$$G_A = E - F_{CLEAR} \tag{2}$$

The global/annual average value of F_{CLEAR} is 265 Wm^{-2} (Harrison et al. 1990), so that G_A is 125 Wm^{-2}. As noted in the introduction, G_A thus provides the largest contribution to the greenhouse effect G, the remaining 30 Wm^{-2} coming from the cloud longwave radiative forcing (Harrison et al. 1990).

It is convenient to use normalised quantities in order to remove the strong temperature

dependence. Raval and Ramanathan (1989) do this by dividing G and G_A by E. In this paper, we use the following normalised measure of the clear-sky greenhouse effect, introduced by Stephens and Greenwald (1991):

$$\mathcal{G} = E / F_{CLEAR} \quad (3)$$

In practice, plots of $\mathcal{G}$ are very similar in appearance to those of the corresponding quantity g, introduced by Raval and Ramanathan (1989).

The contrasting roles of atmospheric temperatures and humidities in the clear-sky greenhouse effect may be illustrated with the help of a simple model. The model is introduced to provide a framework with which to interpret the results shown later, but it is not used in the simulations themselves. Nevertheless, it contains the essential physics which accounts for the seasonal variations, as will be shown later.

The simple model represents the atmosphere as a single, non-scattering layer with emissivity ε_A (Figure 1).The flux emitted upwards from the surface, σT_S^4, is partially absorbed by the atmosphere, so that $(1- \varepsilon_A)\sigma T_S^4$ is transmitted to space. The atmosphere emits $\varepsilon_A \sigma T_A^4$ (where T_A is the mean atmospheric temperature), both upwards to space and downwards to the surface. The total flux emitted to space is thus:

$$F_{CLEAR} = \varepsilon_A \sigma T_A^4 + (1- \varepsilon_A)\sigma T_S^4 \quad (4)$$

From equation 3, the normalized clear-sky greenhouse effect is:

$$\mathcal{G} = \sigma T_S^4 / (\varepsilon_A \sigma T_A^4 + (1- \varepsilon_A)\sigma T_S^4) \quad (5)$$

$\mathcal{G}$ may be expressed in terms of the parameter g (Raval and Ramanathan 1989):

$$g = \varepsilon_A [1 - (T_A/T_S)^4] \quad (6)$$

Hence:

$$\mathcal{G} = 1 / (1 - g) \quad (7)$$

$$= 1 / (1 - \varepsilon_A [1 - (T_A/T_S)^4]) \quad (8)$$

It is assumed that the emissivity ε_A is proportional to the total column moisture content w. This is obviously a simplification, as in reality F_{CLEAR} depends on the vertical structure of the atmospheric temperatures and humidities, which is employed by SAMSON. Nevertheless, equations 6 to 8 illustrate the essential result that there is a separation between the effects of the atmospheric humidities, as measured by w and represented by ε_A in these equations, and the temperatures, as represented by T_A . Increases in w, and hence in ε_A , lead to increases in $\mathcal{G}$ or g. In contrast, increases in T_A lead to a reduction of the temperature contrast between the atmosphere and surface, and hence to lower values of $\mathcal{G}$.

It is reasonable to expect that the relative importance of w and T_A should depend on location. In the tropics, for example, atmospheric temperatures are relatively uniform, but there are significant geographical variations in $\mathcal{G}$ which are highly correlated with those of w, itself largely controlled by the sea surface temperature (Raval and Ramanathan 1989). Away from the tropics, however, atmospheric temperatures are much more variable and, as will be shown, exert a much more powerful control over $\mathcal{G}$ than at low latitudes.

Details of data sources and simulations

The period chosen for this study covers the 12 months from March 1988 through to February 1989, because of the availability of new retrievals of w produced by Greenwald et al. (1993) from SSM/I measurements. Other data used here are the ERBE values of F_{CLEAR} (Harrison et al. 1990) and the National Meteorological Center's blended SSTs (Reynolds 1988). The study is restricted to the ice-free oceans, as in Slingo and Webb (1992), because this minimises problems in defining the surface temperature required to calculate E and also because the SSM/I data are only available over this domain.

The simulations used initialised analyses from the operational archive at the European Centre for Medium Range Weather Forecasts (ECMWF). Since September 1986, temperature

and specific humidity have been available on the model's 19 layer hybrid grid. These data were used directly in the simulations, along with the analysed surface pressure, reducing significantly the amount of vertical interpolation in SAMSON. In all other respects, the data were processed as described by Slingo and Webb (1992). The monthly mean clear-sky emission from the top of the atmosphere was calculated over the ice-free oceans at an horizontal resolution of 2.5 degrees. This was done by running the radiation code once on each 'daily' analysis (a mean of four 6-hourly analyses) and then averaging to give a monthly mean. The error from ignoring the diurnal cycle is small (Slingo and Webb 1992).

Comparison of SAMSON with ERBE and SSM/I

The differences between the ERBE values of F_{CLEAR} and the SAMSON simulations are shown in Fig. 2 for four selected months (April, July and October 1988 and January 1989). The distribution and magnitude of these differences are similar to those found by Slingo and Webb (1992) for the end of the period they studied (October 1986). Positive values of at most slightly more than 10 Wm^{-2} are seen in the sub-tropics, with negative values at the highest latitudes. Overall, there is a positive difference of 3.1 Wm^{-2}, averaged over the four months.

The difference pattern shown in Fig. 2 is consistent with the well known tendency for the ECMWF analyses to be too moist in the sub-tropics (Slingo and Webb 1992). Figure 3 shows the difference between the values of w from the ECMWF analyses used by SAMSON and those retrieved by Greenwald et al. (1993) from the SSM/I data. This comparison clearly shows the ECMWF analyses to be too moist over the sub-tropical stratocumulus regions, consistent with the positive differences evident in Fig. 2. However, Fig. 3 also shows significant differences over the Indian and West Pacific oceans, which are not so well correlated with Fig. 2. Over the rest of the oceans, the analyses are close to the SSM/I retrievals. The mean difference between the ECMWF and SSM/I values of w is 2.4 kg m^{-2}.

Liu et al. (1992) also show difference maps between their own retrievals of w from

SSM/I and the ECMWF analyses (their Plate 5). Over the sub-tropical stratocumulus regions there is good agreement with Fig. 3, but the patterns over the Indian and West Pacific oceans are significantly different. It is possible that this is due to the fact that Liu et al. used a different version of the ECMWF analyses to that employed here, but the most likely explanation is differences between the retrieval algorithms.

It is clearly worth exploring whether the SAMSON simulations might be improved by incorporating information from the new SSM/I retrievals. This was done by adjusting the ECMWF humidities by the same fractional amount at all levels, so that w agreed with the values retrieved from SSM/I. Figure 4 shows the effect on the F_{CLEAR} differences compared with ERBE. The globally meaned difference is reduced (from 3.1 to 1.8 Wm^{-2}) and there is a clear improvement in the stratocumulus regions, compared with Fig. 2. Elsewhere, it is not obvious that constraining the analyses to be consistent with SSM/I is beneficial. There are several areas where the general increase in the simulated fluxes produces larger negative differences compared with ERBE, for example over the West Pacific ocean in October 1988. In addition, many features of the patterns in Fig. 2 are not removed, such as over the West and central Pacific ocean in January 1989. These results suggest that errors in w in the ECMWF analyses are by no means the only reason for the differences between the SAMSON simulations and ERBE.

In view of these results, it was decided not to adjust the ECMWF analyses for the following investigation. The differences evident in Fig.2 are in any case much smaller than the magnitude of the seasonal variations shown in the next section, so the simulations are more than adequate for the purpose of this paper. This decision has the additional advantage that the data employed in SAMSON are as independent as possible from the satellite data (neither ERBE nor SSM/I data were assimilated into the ECMWF analyses during this period).

Greenhouse effect scatter plots

The normalized clear-sky greenhouse effect G is plotted against w in Fig. 5, for the near-equinox months of April and October 1988. Results are shown from the satellite data (using ERBE and SSM/I) and also from SAMSON. The plots show the strong correlation noted by previous authors, as well as a tendency for a change in slope for values of w below about 20 kgm^{-2}. The relationship between G and w from SAMSON is close to that from the satellite data, although the latter show the enhanced scatter which is to be expected from the merger of two independent satellite datasets.

The character of the plots changes when the near-solstice months of July 1988 and January 1989 are considered (Fig. 6). There is now a marked branching at low values of w. In each case, it is the winter hemisphere branch which provides the higher values of G, with the northern and southern hemispheres alternating from July to January. As in Fig. 5, there is less scatter in the SAMSON plots, which show the branching most clearly. There is also some missing data from ERBE in July 1988. Examination of the scatter plots for all the months shows that the branches for each hemisphere behave independently, with low values of G in summer, increasing through autumn to a maximum in winter and then declining to the summer value again. The two branches cross over in spring and autumn, producing the apparently single relationship shown on the plots in Fig. 5.

Is this behaviour due to the associated changes in w? To examine this possibility, w is plotted against SST in Fig. 7, both from the satellite data (SSM/I) and from SAMSON (i.e. the ECMWF analyses). This figure shows the familiar increase of w with SST, which is largely controlled by the Clausius-Clapeyron equation, modulated by the effects of atmospheric moisture convergence (Stephens 1990). It also shows that w displays well defined branches which are at least as coherent as those for G shown in Fig. 6. In this case, however, w is higher in the summer hemisphere than in the winter hemisphere. This behaviour is to be expected from

thermodynamic arguments, given the higher atmospheric temperatures in summer.

The seasonal variations of w evident in Fig. 7 are of the *wrong sign* to explain the seasonal variations of G shown in Fig. 6. An increase in w in summer should lead to an increase in G, because water vapour is the primary greenhouse gas and an increase in w should therefore enhance the greenhouse effect, as shown by equations 6 to 8. This may not be true if there is a radical re-distribution of moisture in the vertical from winter to summer, but the analysis in the following section shows that this does not take place. From Fig. 7, one would expect G to be highest in summer, but Fig. 6 shows that in fact this is the time of year when G is smallest.

It will be shown in the following section that the seasonal variations in G, as manifested by the branches in Fig. 6, are dominated by the seasonal variations in the atmospheric *temperatures*, rather than the moisture contents. It is first necessary to minimise the confusing influence of moisture variations in Fig. 6, by removing w from the abscissa and replacing it by SST. As noted above, there are large seasonal variations in w at high latitudes which are of the wrong sign to explain the seasonal variations in G, so it is clearly inappropriate to use w as the independent variable.

When G is plotted against SST (Fig. 8), the branches are still clearly visible in the SAMSON plots, but they are somewhat obscured in the satellite plots by the scatter in the ERBE data (and to a lesser extent by missing data). The outlying points with low values of SST but high values of G are where the ERBE data were obtained when the sea surface was covered with sea-ice, but which were classified as being, on average through the month, open water in the blended SST data. For these points, F_{CLEAR} is thus anomalously low compared with the calculated surface emission, leading to a spuriously high value of G (see equation 3). These points are excluded from Fig. 6, because the SSM/I data do not extend far enough polewards.

The coherent features in the summer and winter branches are examined further in Fig. 9, which shows data for June 1988, a month with particularly good agreement between the

plots derived from the ERBE data and those from SAMSON. The data from the two hemispheres are shown separately, which facilitates comparison between the ERBE and SAMSON plots. The reader is encouraged to do this by photocopying one set of plots and superimposing it over the other to create a 'flip-chart'. This demonstrates the close agreement between the two (apart from the scatter in the ERBE data), which even extends to the few points in the northern hemisphere with high SSTs but low values of $\mathcal{G}$. These are over locations such as the Persian Gulf, where the atmosphere is relatively dry and warm because of the influence of the surrounding deserts. The only notable area of disagreement is the slight overestimate by SAMSON in the southern (winter) hemisphere, for SSTs in the range 290-300K. This is a consequence of the underestimate of F_{CLEAR} by about 5 Wm^{-2} (compared with ERBE) in the sub-tropics (cf Fig. 2), due to the moist bias of the ECMWF analyses in this region (cf Fig. 3).

Figure 9 emphasizes the difference in slope between the plots from the two hemispheres, the effect of which extends almost to the highest values of the SST. The southern hemisphere plot using the ERBE data is particularly striking, showing a sudden change in the slope at an SST of about 300K, above which the greatly enhanced upper tropospheric humidities in the ITCZ produce a steep rise in $\mathcal{G}$. This enhancement of the slope for the highest SSTs is the phenomenon referred to by Ramanathan and Collins as the 'super greenhouse effect'. In these regions, the value of $\mathcal{G}$ is clearly controlled by w, and hence by the SST, rather than by atmospheric temperatures.

Sensitivity to changes in atmospheric temperatures and humidities

In order to determine the factors which control the seasonal variations in the clear-sky greenhouse effect at middle and high latitudes, sensitivity experiments were performed with SAMSON using the data for June 1988. The atmospheric temperatures and humidities were first averaged, to reduce the scatter evident in the previous figures. SST intervals of width 1K

were defined and all the profiles within each interval were averaged for each hemisphere. SAMSON was run for these average profiles, and also for mixed profiles constructed from the summer hemisphere temperatures and the winter hemisphere humidities. By comparing the simulations for the mixed profiles with those for summer and winter, it will be shown that the seasonal variations in $\mathcal{G}$ are mainly due to the seasonal variations in the atmospheric temperatures, as opposed to those in the humidities.

Figure 10 shows the relationship between $\mathcal{G}$ and SST from these experiments, overlayed on the simulations previously displayed in Fig. 9. The simulations with the average profiles succesfully capture the shape of the branches, while removing the scatter which arises from the details of individual profiles in the analyses. The open squares in the lower branch show the values of $\mathcal{G}$ for the summer hemisphere. The open triangles are for the mixed profiles, which have lower values of $\mathcal{G}$ than the summer profiles. This is to be expected; reducing the humidities to their winter values whilst keeping the temperatures at their summer values should indeed weaken the greenhouse effect. Comparing the open triangles with the open squares in the upper branch shows the effect of now reducing the atmospheric temperatures to their winter values. There is a substantial rise in the value of $\mathcal{G}$, to well above the corresponding value in the summer hemisphere. This demonstrates that the temperature differences between the winter and summer hemispheres dominate the seasonal variations in $\mathcal{G}$, leading to an enhanced clear-sky greenhouse effect in winter, despite the lower values of w.

At a sea surface temperature of about 288K, the branches disappear as the winter and summer values of $\mathcal{G}$ converge, yet the value of $\mathcal{G}$ for the mixed profiles remains lower. This suggests that, in this region of the scatter plot, differences between the temperature and humidity profiles in winter and summer are of roughly comparable importance. Drying the summer profile with the winter humidities thus reduces $\mathcal{G}$, but cooling this mixed profile to recover the winter temperatures increases $\mathcal{G}$ to roughly the same value as in summer.

Further insights may be gained by examining the results for four values of SST in greater detail. These are shown by the vertical lines in Fig. 10, labelled a through d. Tephigrams for the corresponding average summer and winter profiles are shown in Fig. 11. Within the boundary layer, the summer profiles have inversions whereas the winter profiles are more unstable. Above about 700hPa, however, the shapes of the profiles are similar and the lapse rates of temperature and humidity in the middle and upper troposphere are not substantially different in summer and winter. The main difference between summer and winter in this region is that the profiles are displaced to the right in summer, when both temperatures and humidities are higher than in winter. This displacement could be interpreted as a change in the mean lapse rate from the surface to the tropopause, but this would mis-represent the different behaviour above and below 700hPa. The difference between the summer and winter profiles lies not so much in the mean tropospheric lapse rate as in the mean temperatures and humidities in the middle and upper troposphere.

Table 1 lists the values of w, F_{CLEAR} and G for the summer, mixed and winter profiles at each of the four SSTs. The dominance of the seasonal variations in atmospheric temperatures at the lowest SST value is illustrated by the fact that the value of w for the winter profile is almost half that in summer (6.7 kgm^{-2} compared with 11.0 kgm^{-2}), yet the value of G is higher (1.42 compared with 1.31). Within each hemisphere, however, G increases with both SST and w until the highest SST value is reached, when the hemispheres become indistinguishable.

Discussion

At low latitudes, variations in the clear-sky greenhouse effect G are controlled largely by variations in the total column moisture content w of the atmosphere, with variations in atmospheric temperatures of lesser importance. Seasonal variations are small, but there are significant geographical variations in both G and w, both of which are largely controlled by the SST

distribution.

In contrast, at high latitudes both G and w exhibit strong seasonal variations. When each variable is plotted against SST, the points separate into distinct branches corresponding to the summer and winter hemispheres. The highest values of w occur in summer, which is to be expected on thermodynamic grounds because this is when the atmospheric temperatures are highest. However, the clear-sky greenhouse effect is highest in winter, which cannot be explained by the variations in w. The clear-sky greenhouse effect variations are controlled instead by the seasonal changes in atmospheric temperatures, which are strong enough to overcome the opposing effect of the moisture variations. The colder atmosphere in winter increases the temperature contrast between the atmosphere and surface, enhancing the greenhouse effect in spite of the lower humidities.

The SAMSON simulations, including those for the mixed profiles, make use of the full vertical structure of temperature and humidity in the ECMWF analyses. But the results are also consistent with the simple model (equations 4-8), in which the atmosphere is represented by a single layer with temperature T_A and emissivity ε_A. This is obviously a gross simplification of the real structure, but the equations contain the essential dependence on temperature and humidity which is present in the simulations. Following the discussion of Fig. 11, T_A may be interpreted as the average radiating temperature of the middle and upper troposphere. This region makes the dominant atmospheric contribution to G at middle and high latitudes. The lower troposphere is less important at these latitudes, so the temperature and humidity differences below about 700hPa shown in Fig. 11 have very little influence on the seasonal variations in G.

While the temporal variations in temperature at a given location control the phase of the seasonal cycle in the clear-sky greenhouse effect, the importance of systematic changes in w with latitude should not be underestimated. Consider the latitudinal changes in G for a given

time of year, for example from the SAMSON simulations for July 1988 (Fig.8). At low latitudes G is a maximum, because the temperature contrast between the surface and the middle troposphere is a maximum and because w is also largest (Fig. 7). As one moves towards each pole, w decreases (Fig. 7), which tends to reduce G. However, in the winter hemisphere the mean atmospheric temperature decreases much faster than in the summer hemisphere. In the absence of other changes, this would increase G as the winter pole is approached. The net result of the latitudinal variations in w and temperature is therefore that G decreases towards the winter pole at a much slower rate than it does towards the summer pole (Fig. 8). The slope of the two branches in Fig. 8 is thus controlled by the latitudinal variations in **both** w and temperature. In addition, the asymmetry in the positions of the winter and summer branches in July and January reflects the asymmetry in these quantities between the two hemispheres.

The use of the simple model in this discussion is somewhat qualitative, although the conclusions are supported by the sensitivity experiments with SAMSON. This employs the full detail of the vertical structure of the atmospheric temperatures and humidities, as represented in the operational analyses. A valuable exercise would be to investigate whether the simple model is capable of explaining quantitatively the features investigated here. The model requires values for the bulk quantities discussed above (SST, w and a mean atmospheric temperature). Such an investigation would enable an assessment of the importance of, for example, details of the vertical distribution of moisture and temperature, compared with the bulk quantities such as w.

Climate models should be able to reproduce the seasonal variations in the quantities examined in this paper. Comparison of the output of these models with the satellite and SAMSON plots should therefore provide valuable information on the simulation both of the hydrological cycle and of the clear-sky greenhouse effect. Such comparisons are now in progress with the Hadley Centre model.

The work reported in this paper was presented at a Workshop on Radiation in GCMs, held at the Hadley Centre on 24-25 March 1993. A presentation by Dr. J.-P. Duvel showed that he had independently worked on this topic and had arrived at similar conclusions. His work will be reported in a separate paper.

Acknowledgements. Thanks are due to J.M. Gregory, S.F.B. Tett and I. Edmond for their development of data analysis and graphics software used throughout this study. The work at the Hadley Centre was funded by the U.K. Department of the Environment under contract PECD 7/12/37. G.L. Stephens was supported by NASA Grant NAG8-876 and by NOAA Grants NA90AA-D-AC822 and NA90RAH-00077.

References

Duvel JP, Bréon FM (1991) The clear-sky greenhouse effect sensitivity to a sea surface temperature change. J Climate 4: 1162-1169

Greenwald TJ, Stephens GL, Vonder Haar TH, Jackson DL (1993) A physical retrieval method of liquid water over the global oceans using SSM/I observations. J Geophys Res: in press

Harrison EF, Minnis P, Barkstrom BR, Ramanathan V, Cess RD, Gibson GG (1990) Seasonal variation of cloud radiative forcing derived from the Earth Radiation Budget Experiment. J Geophys Res 95: 18687-18703

Liu WT, Tang W, Wentz FJ (1992) Precipitable water and surface humidity over global oceans from special sensor microwave imager and European Center for Medium range Weather Forecasts. J. Geophys Res 97: 2251-2264

Ramanathan V, Collins W (1991) Thermodynamic regulation of ocean warming by cirrus clouds deduced from observations of the 1987 El Niño. Nature 351: 27-32

Raval A, Ramanathan V (1989) Observational determination of the greenhouse effect. Nature 342: 758-761

Reynolds RW (1988) A real-time global sea surface temperature analysis. J Climate 1: 75-86

Senior CA, Mitchell JFB (1993) Carbon dioxide and climate: the impact of cloud parameterization. J Climate 6: 393-418

Slingo A, Webb MJ (1992) Simulation of clear-sky outgoing longwave radiation over the oceans using operational analyses. Quart J Roy Meteorol Soc 118: 1117-1144

Stephens GL (1990) On the relationship between water vapor over the oceans and sea surface temperature. J Climate 3: 634-645

Stephens GL, Greenwald TJ (1991) The Earth's radiation budget and its relation to atmospheric hydrology: 1. Observations of the clear sky greenhouse effect. J Geophys Res 96: 15325-15340

Table 1. Characteristics of the points selected from Fig. 10 to illustrate the relative importance of changes in atmospheric temperatures and humidities on the seasonal variations in the clear-sky greenhouse effect. SST is the sea surface temperature, w is the total column moisture content, F_{CLEAR} is the clear-sky emission from the top of the atmosphere and G is the normalized clear-sky greenhouse effect, as defined by equation 3.

Profile	SST (K)	w (kgm^{-2})	F_{CLEAR} (Wm^{-2})	G
Summer	272.5	11.0	238.4	1.31
Mixed	272.5	6.7	243.8	1.28
Winter	272.5	6.7	220.6	1.42
Summer	280.5	18.9	249.4	1.41
Mixed	280.5	11.6	258.8	1.36
Winter	280.5	11.6	239.5	1.47
Summer	288.5	26.8	263.4	1.49
Mixed	288.5	18.1	273.5	1.44
Winter	288.5	18.1	261.0	1.50
Summer	296.5	33.0	281.2	1.56
Mixed	296.5	29.1	286.2	1.53
Winter	296.5	29.1	284.0	1.54

Figure captions

Fig. 1. Schematic of the contributions to the clear-sky longwave fluxes for a one-layer model of the atmosphere (see text for discussion)

Fig. 2. Differences between the ERBE and SAMSON clear-sky emission from the top of the atmosphere (F_{CLEAR}) for April, July and October 1988 and January 1989. The contour interval is 5 Wm^{-2}. Values greater than 5 Wm^{-2} and 10 Wm^{-2} are hatched with opposing patterns

Fig. 3. Differences between the ECMWF and SSM/I total column moisture content of the atmosphere (w) for April, July and October 1988 and January 1989. The contour interval is 5 kgm^{-2}. Values greater than 5 kgm^{-2} and 10 kgm^{-2} are hatched with opposing patterns

Fig. 4. Differences between the ERBE and SAMSON clear-sky emission from the top of the atmosphere (F_{CLEAR}) for April, July and October 1988 and January 1989, after the ECMWF humidities have been adjusted so that the total column moisture content w is the same as that from SSM/I. The contour interval is 5 Wm^{-2}. Values greater than 5 Wm^{-2} and 10 Wm^{-2} are hatched with opposing patterns

Fig. 5. Scatter plots of the normalized clear-sky greenhouse effect G against the total column moisture content of the atmosphere w in kgm^{-2} for April and October 1988, from ERBE and SSM/I (a and c) and from SAMSON (b and d)

Fig. 6. Scatter plots of the normalized clear-sky greenhouse effect G against the total column

moisture content of the atmosphere w in kgm^{-2} for July 1988 and January 1989, from ERBE and SSM/I (a and c) and from SAMSON (b and d). Northern hemisphere points are plotted with an open square and southern hemisphere points are plotted with a plus sign

Fig. 7. Scatter plots of the total column moisture content of the atmosphere w in kgm^{-2} against the sea surface temperature (SST) in K for July 1988 and January 1989, from SSM/I (a and c) and from the ECMWF analyses used in SAMSON (b and d). Northern hemisphere points are plotted with an open square and southern hemisphere points are plotted with a plus sign

Fig. 8. Scatter plots of the normalized clear-sky greenhouse effect G against the sea surface temperature (SST) in K for July 1988 and January 1989, from ERBE (a and c) and from SAMSON (b and d). Northern hemisphere points are plotted with an open square and southern hemisphere points are plotted with a plus sign

Fig. 9. Scatter plots of the normalized clear-sky greenhouse effect G against the sea surface temperature (SST) in K for June 1988 from ERBE (a and c) and from SAMSON (b and d). Northern hemisphere points are plotted separately in the upper frames and southern hemisphere points are plotted separately in the lower frames

Fig. 10. Scatter plot of the normalized clear-sky greenhouse effect G against the sea surface temperature (SST) in K for June 1988 from SAMSON. The open squares denote the values of G when SAMSON is run with the mean temperature and humidity profiles obtained by averaging the data from all the points in each hemisphere within a 1K interval around a given value of SST. The open triangles denote the values of G when SAMSON is run with the mean tem-

peratures from the summer points (the lower branch) and the mean humidities from the winter points (the upper branch). Tephigrams for the mean winter and summer profiles for the SSTs marked a to d are shown in Fig. 11 and the values of various quantities for these profiles are listed in Table 1.

Fig. 11. Tephigrams of the mean profiles of temperature and dew point temperature for the points marked a to d in Fig. 10. The summer hemisphere temperatures and dew points are plotted as the continuous bold lines and the winter hemisphere temperatures and dew points are plotted as the dashed bold lines. The temperature profile is to the right of the corresponding dew point temperature profile. The dotted lines which are nearly horizontal are the isobars, plotted every 100 hPa, with the 1000hPa isobar emphasized. The solid lines sloping upwards to the right are the isotherms, plotted every 20°C, with the 0°C isotherm shown dashed.

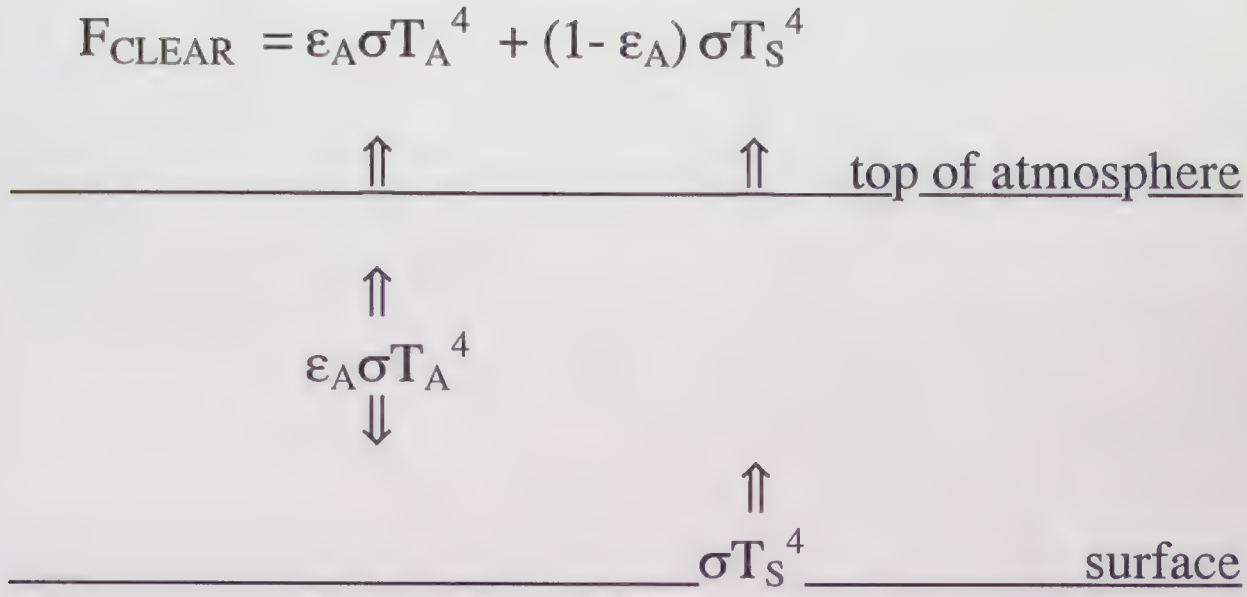
$F_{CLEAR} = \varepsilon_A \sigma T_A^4 + (1 - \varepsilon_A) \sigma T_S^4$
top of atmosphere
$\varepsilon_A \sigma T_A^4$
σT_S^4
surface

Fig. 1

a) Clear-sky OLR April 1988

ERBE minus simulation using ECMWF Analyses

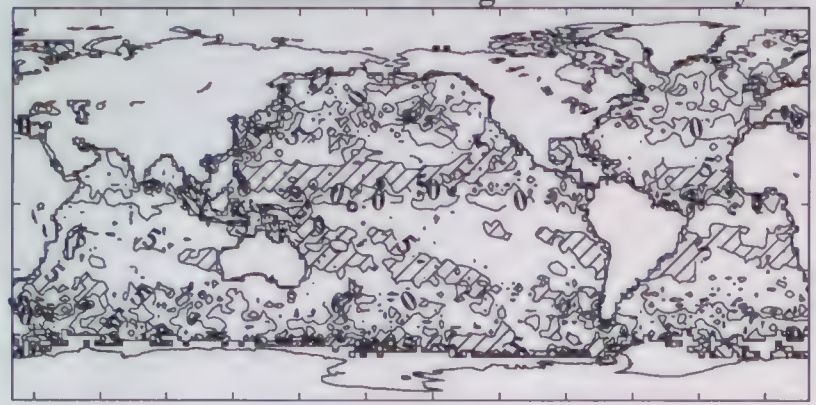

mean= 2.80 rms= 5.58

b) Clear-sky OLR July 1988

ERBE minus simulation using ECMWF Analyses

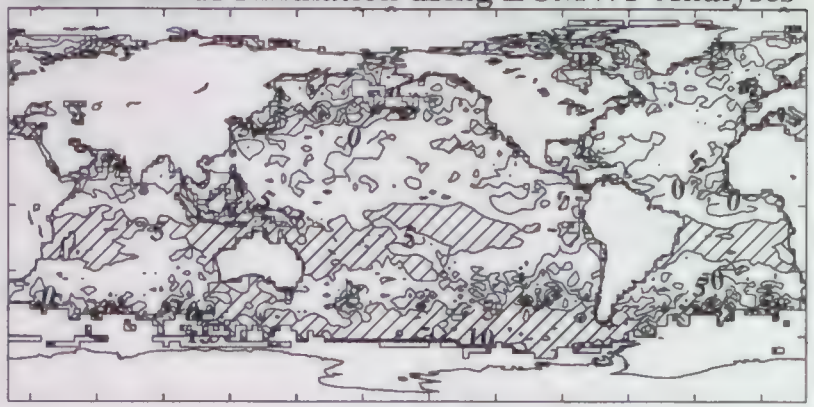

mean= 2.87 rms= 6.55

c) Clear-sky OLR October 1988

ERBE minus simulation using ECMWF Analyses

mean= 3.15 rms= 4.81

d) Clear-sky OLR January 1989

ERBE minus simulation using ECMWF Analyses

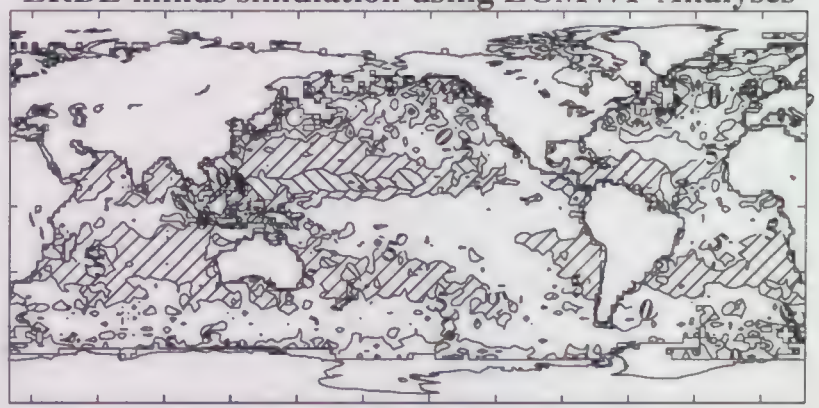

mean= 3.67 rms= 6.48

Fig 2

a) Column Moisture April 1988

ECMWF minus SSM/I

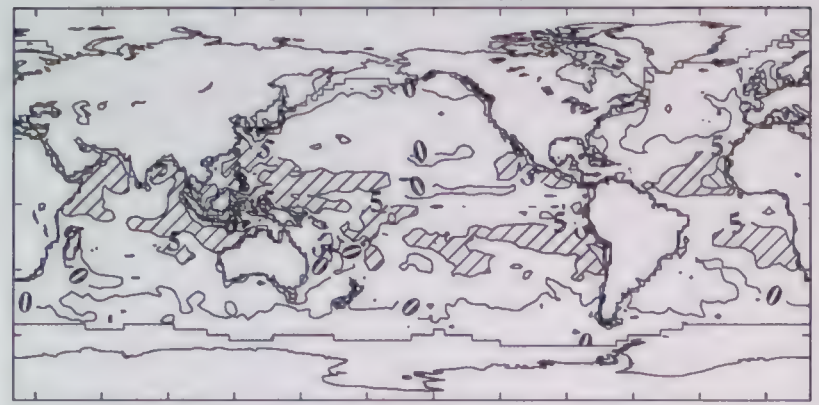

mean= 2.37 rms= 3.81

b) Column Moisture July 1988

ECMWF minus SSM/I

mean= 2.32 rms= 4.00

c) Column Moisture October 1988

ECMWF minus SSM/I

mean= 2.81 rms= 4.21

d) Column Moisture January 1989

ECMWF minus SSM/I

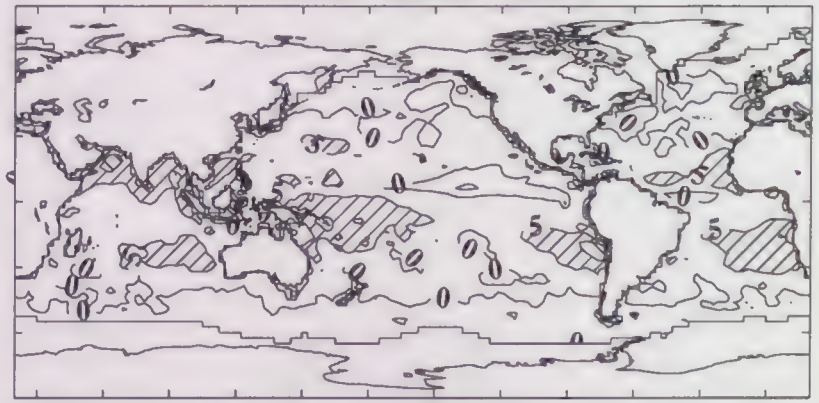

mean= 1.93 rms= 3.56

Fig 3

a) Clear-sky OLR April 1988

ERBE minus simulation using ECMWF Analyses & SSM/I

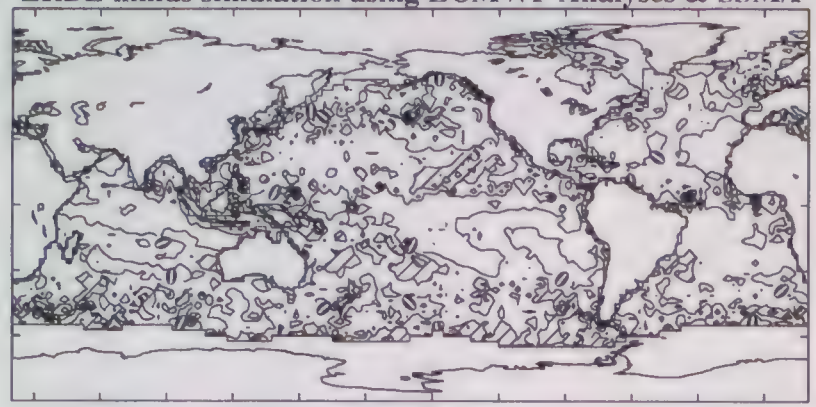

mean= 1.28 rms= 4.23

b) Clear-sky OLR July 1988

ERBE minus simulation using ECMWF Analyses & SSM/I

mean= 1.60 rms= 4.48

c) Clear-sky OLR October 1988

ERBE minus simulation using ECMWF Analyses & SSM/I

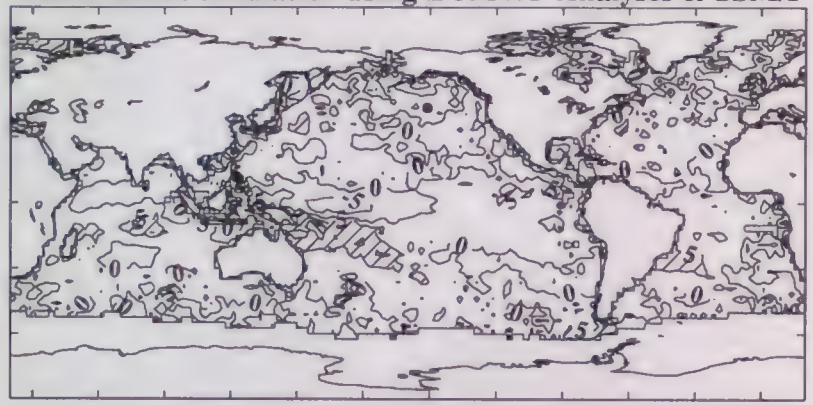

mean= 1.46 rms= 3.44

d) Clear-sky OLR January 1989

ERBE minus simulation using ECMWF Analyses & SSM/I

mean= 2.79 rms= 4.78

Fig 4

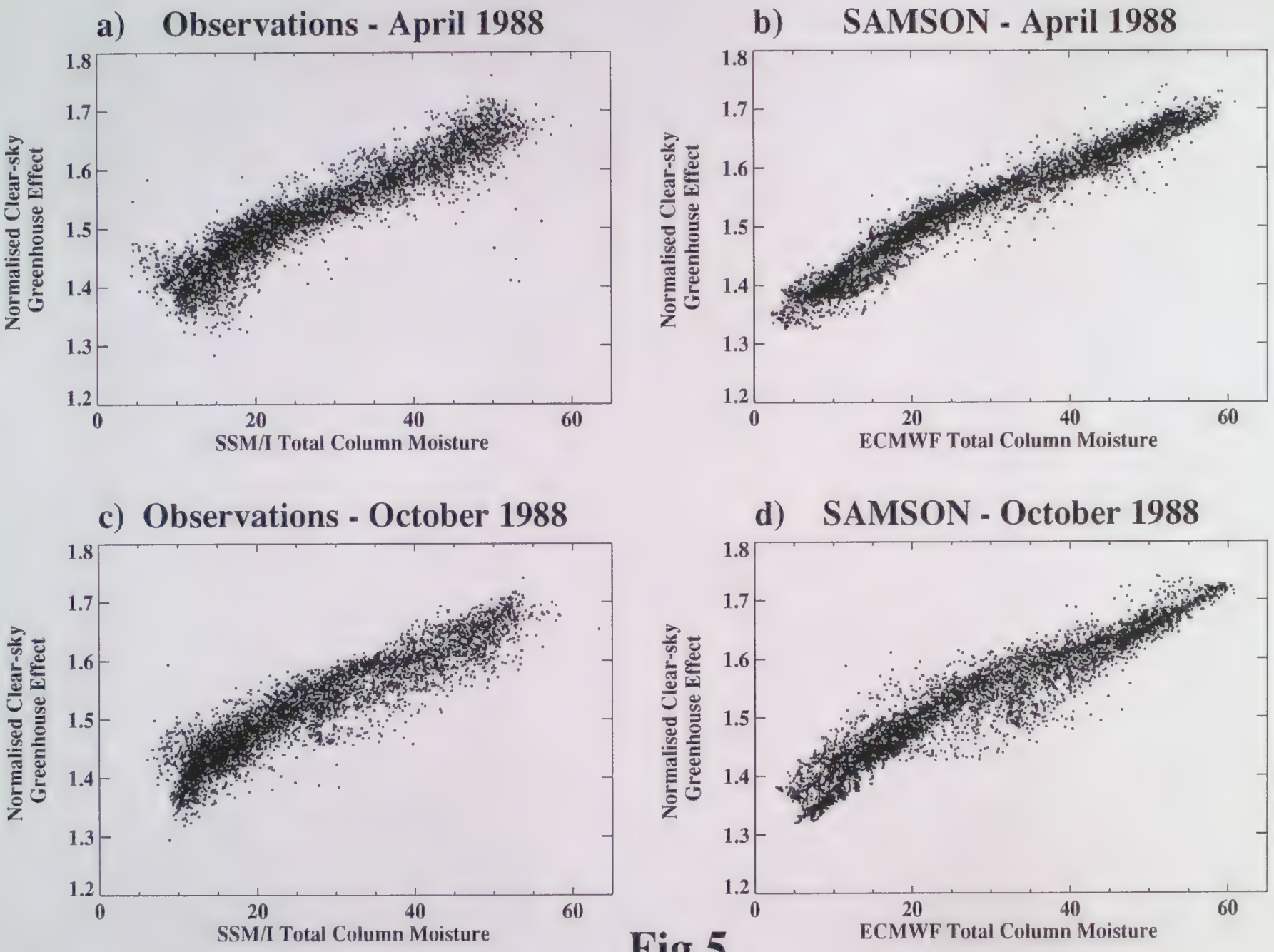
a) Observations - April 1988
b) SAMSON - April 1988
c) Observations - October 1988
d) SAMSON - October 1988
Normalised Clear-sky Greenhouse Effect
SSM/I Total Column Moisture
ECMWF Total Column Moisture
1.2
1.3
1.4
1.5
1.6
1.7
1.8
0
20
40
60

Fig 5

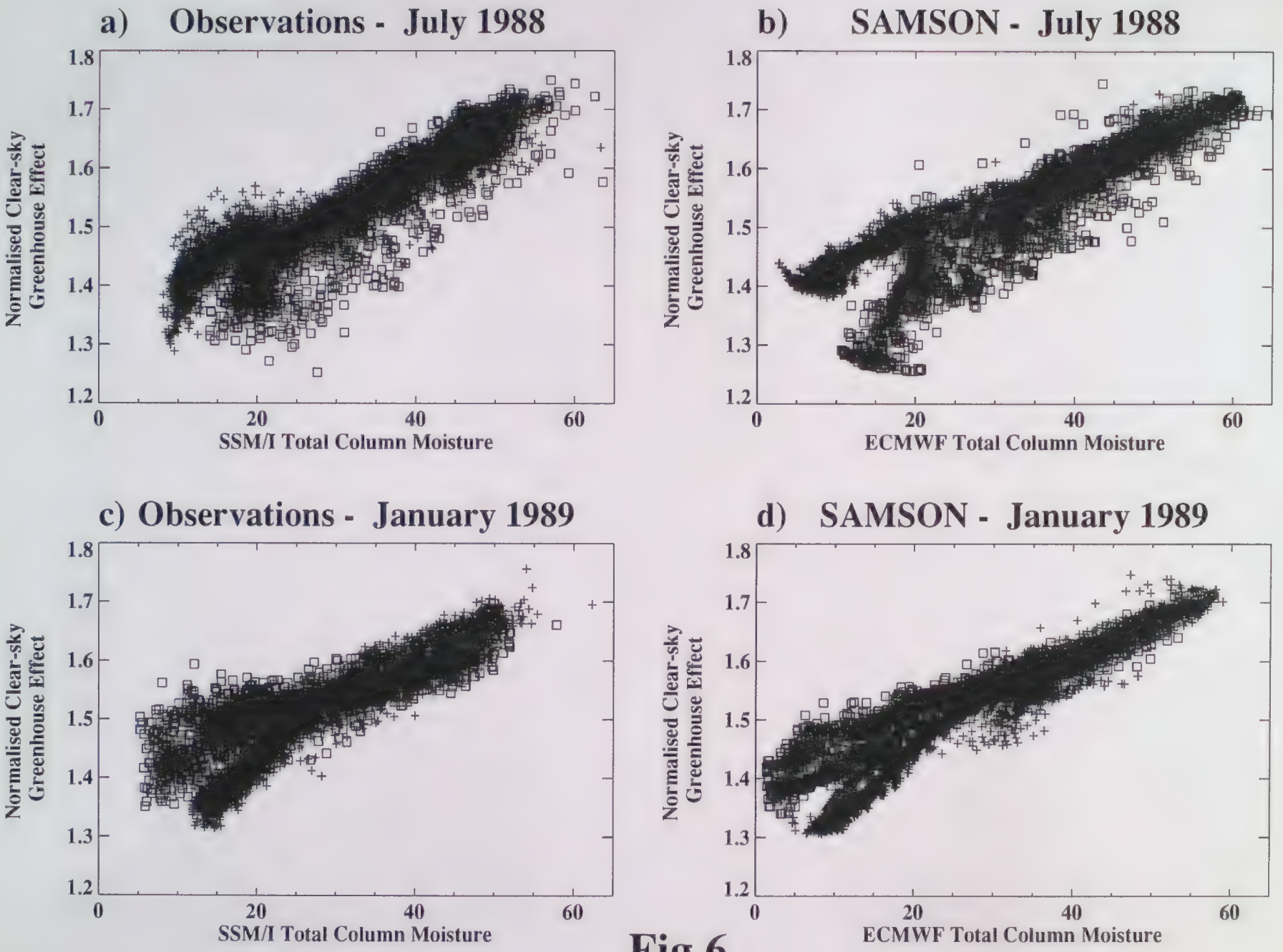
a) Observations - July 1988
b) SAMSON - July 1988
c) Observations - January 1989
d) SAMSON - January 1989
Normalised Clear-sky Greenhouse Effect
SSM/I Total Column Moisture
ECMWF Total Column Moisture
1.2
1.3
1.4
1.5
1.6
1.7
1.8
0
20
40
60

Fig 6

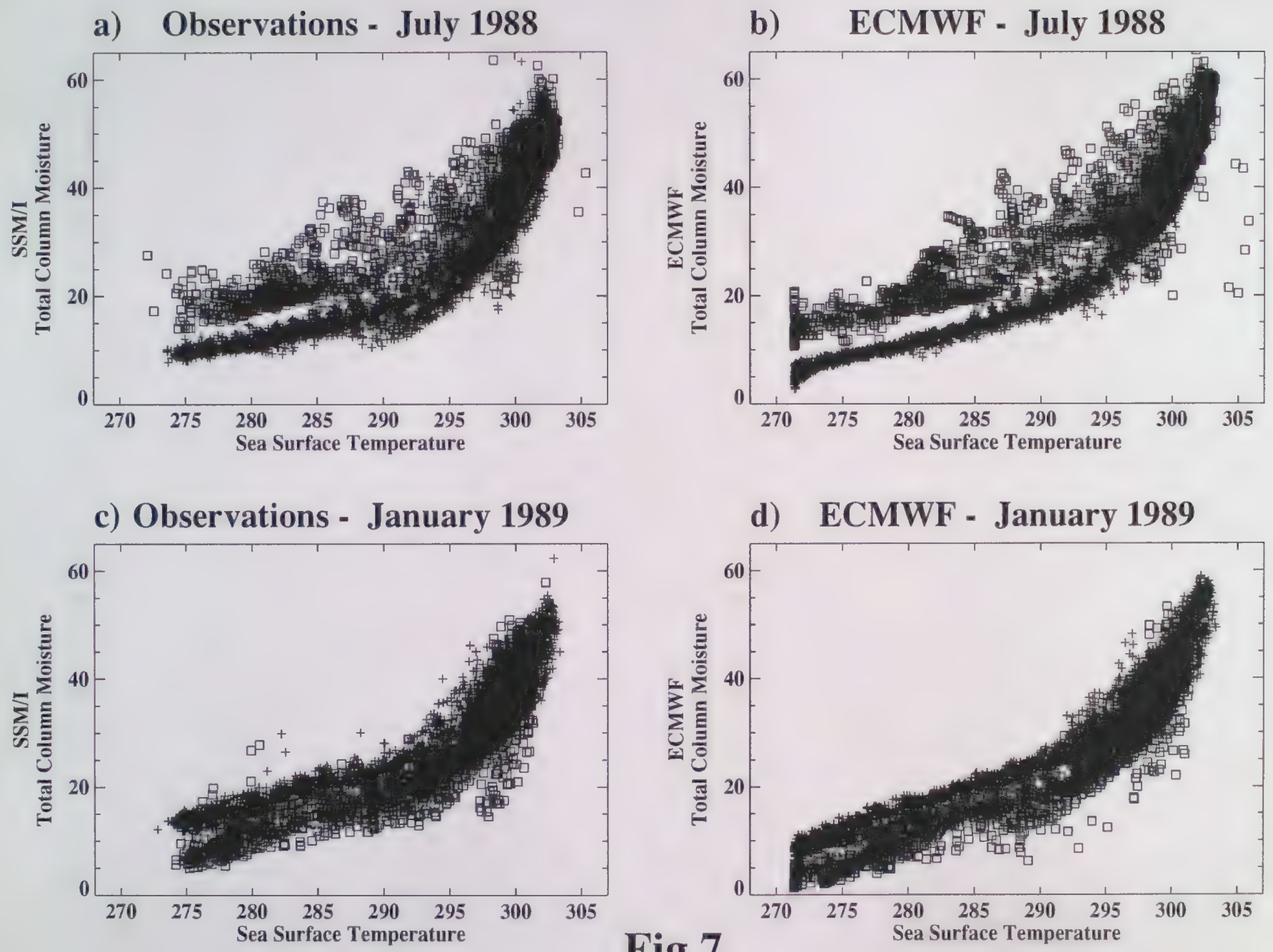
a) Observations - July 1988
b) ECMWF - July 1988
c) Observations - January 1989
d) ECMWF - January 1989
SSM/I Total Column Moisture
ECMWF Total Column Moisture
Sea Surface Temperature
0
20
40
60
270
275
280
285
290
295
300
305

Fig 7

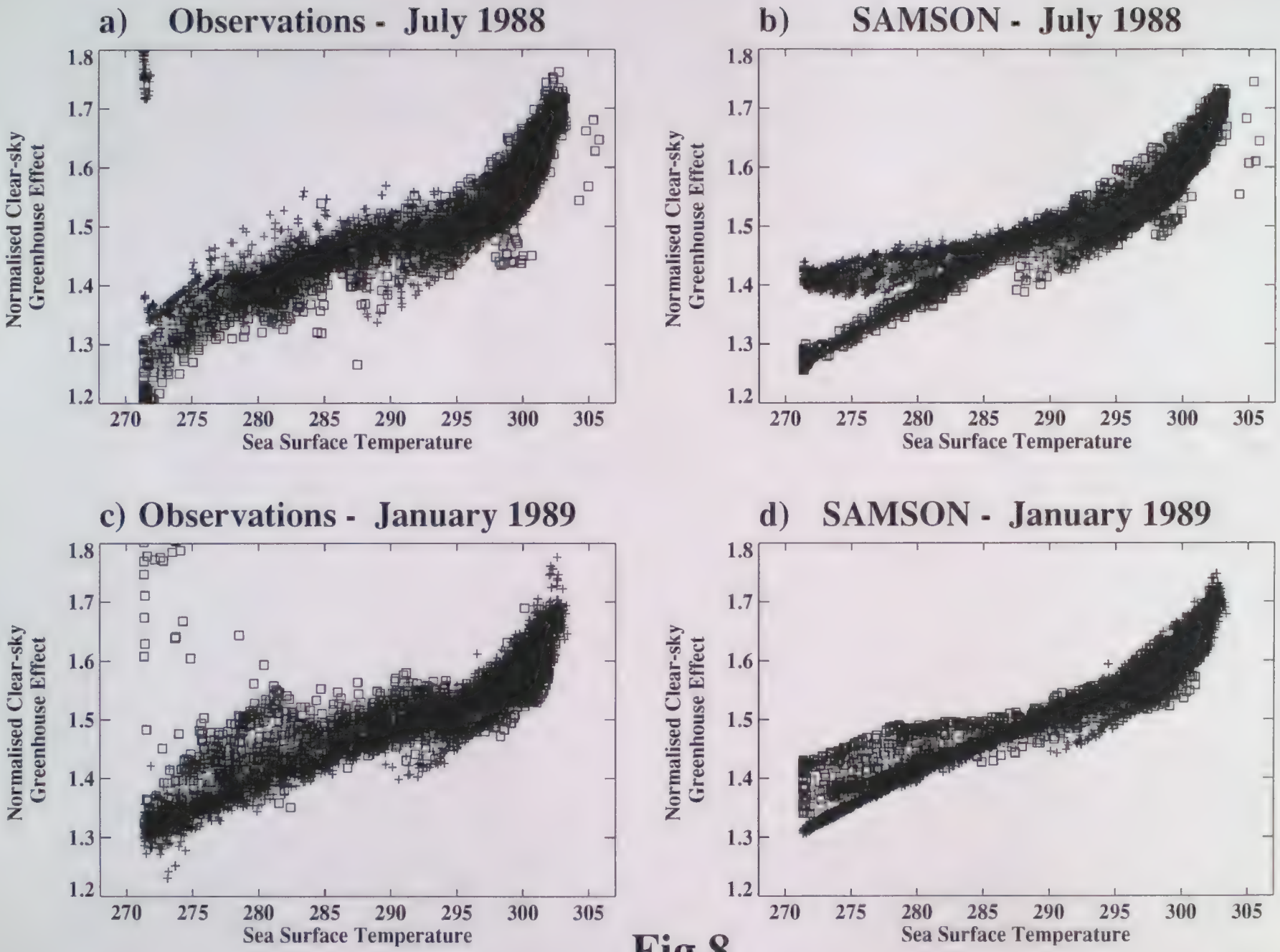
a) Observations - July 1988
b) SAMSON - July 1988
c) Observations - January 1989
d) SAMSON - January 1989
Normalised Clear-sky Greenhouse Effect
Sea Surface Temperature
1.2
1.3
1.4
1.5
1.6
1.7
1.8
270
275
280
285
290
295
300
305

Fig 8

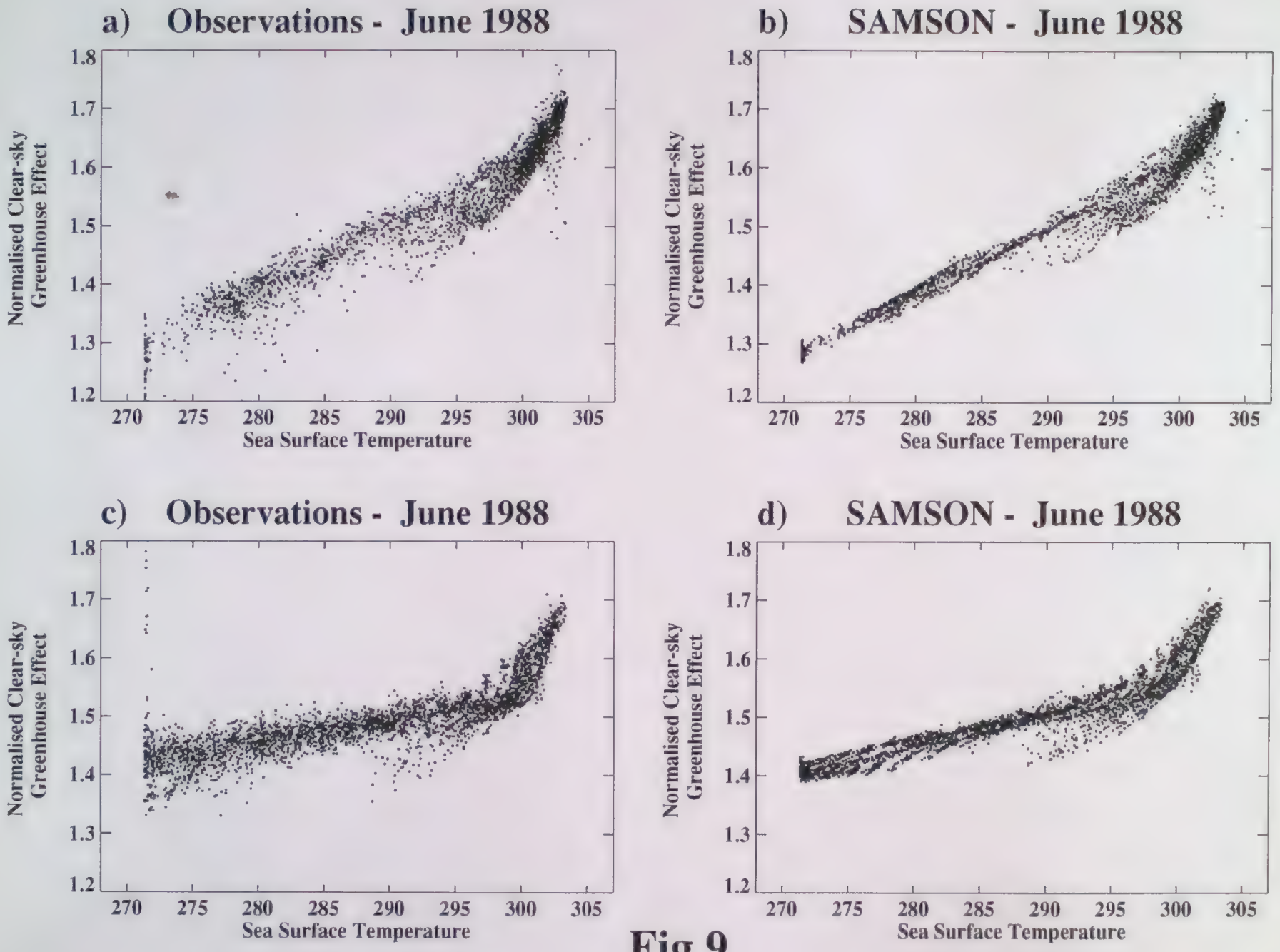
a) Observations - June 1988
b) SAMSON - June 1988
c) Observations - June 1988
d) SAMSON - June 1988
Normalised Clear-sky Greenhouse Effect
Sea Surface Temperature
1.2
1.3
1.4
1.5
1.6
1.7
1.8
270
275
280
285
290
295
300
305

Fig 9

SAMSON - June 1988

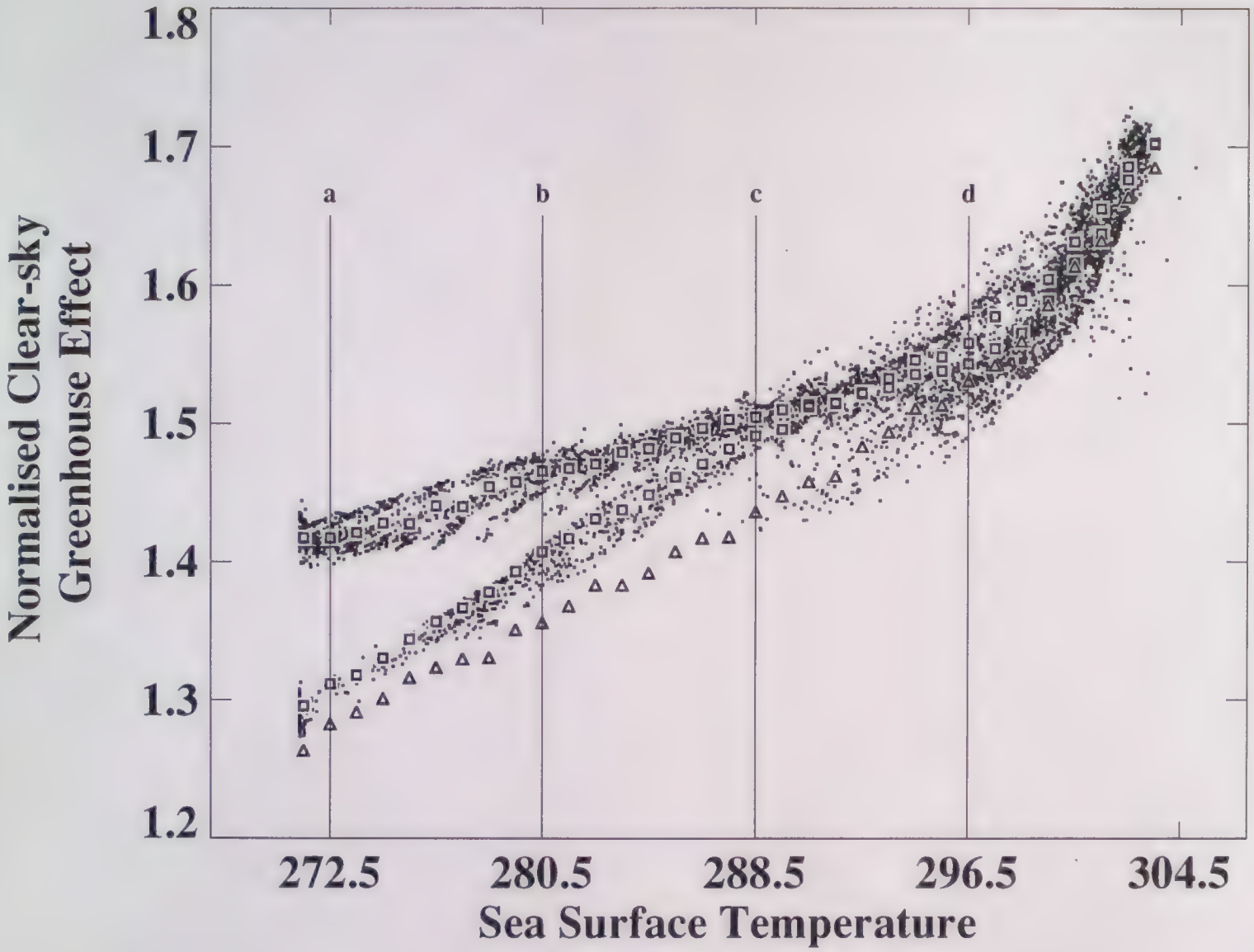

Fig 10

a) Surface Temperature 272.5K

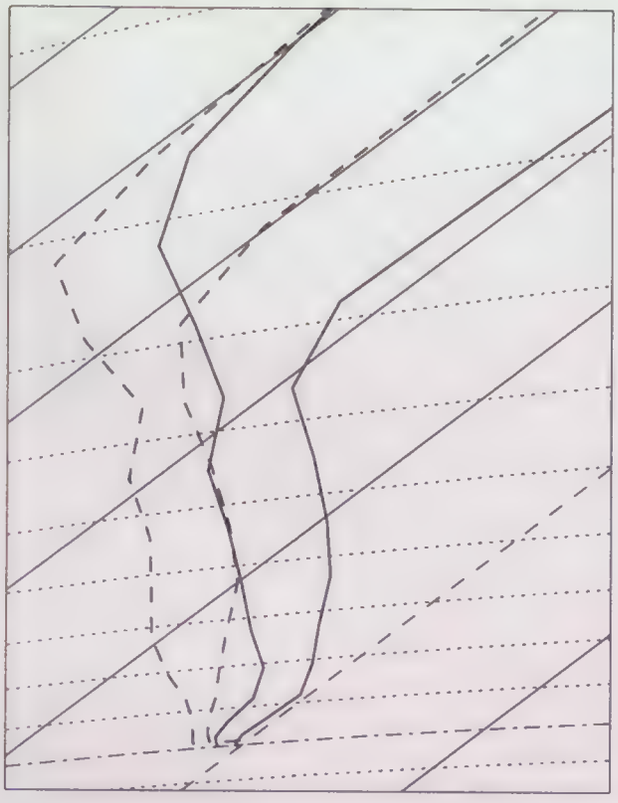

b) Surface Temperature 280.5K

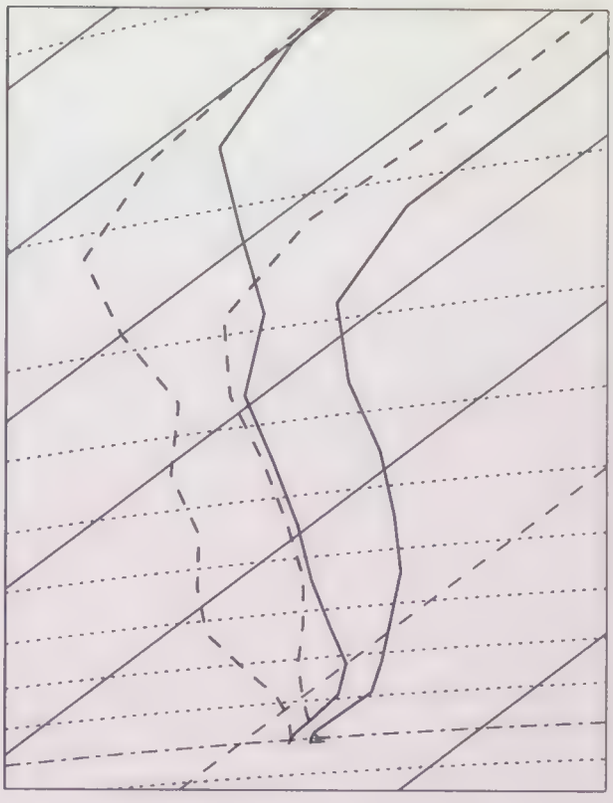

c) Surface Temperature 288.5K

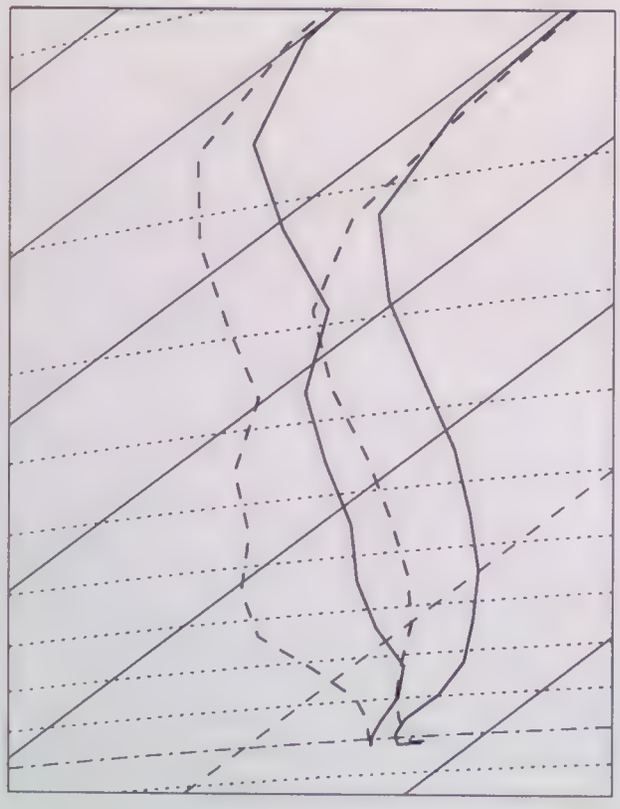

d) Surface Temperature 296.5K

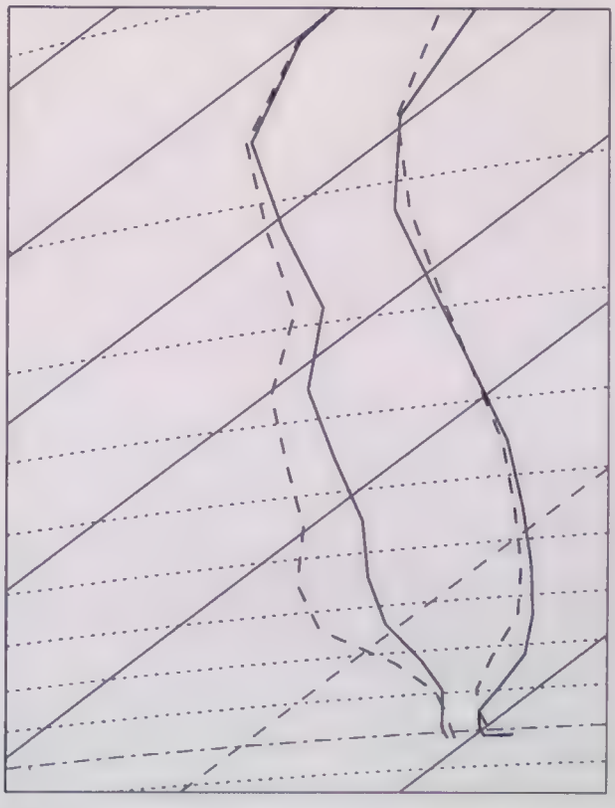

Fig 11

CLIMATE RESEARCH TECHNICAL NOTES

CRTN 1	Oct 1990	Estimates of the sensitivity of climate to vegetation changes using the Penman-Monteith equation. P R Rowntree
CRTN 2	Oct 1990	An ocean general circulation model of the Indian Ocean for hindcasting studies. D J Carrington
CRTN 3	Oct 1990	Simulation of the tropical diurnal cycle in a climate model. D P Rowell
CRTN 4	Oct 1990	Low frequency variability of the oceans. C K Folland, A Colman, D E Parker and A Bevan
CRTN 5	Dec 1990	A comparison of 11-level General Circulation Model Simulations with observations in the East Sahel. K Maskell
CRTN 6	Dec 1990	Climate Change Prediction. J F B Mitchell and Qing-cun Zeng
CRTN 7	Jan 1991	Deforestation of Amazonia - modelling the effects of albedo change. M F Mylne and P R Rowntree
CRTN 8	Jan 1991	The role of observations in climate prediction and research. D J Carson
CRTN 9	Mar 1991	The greenhouse effect and its likely consequences for climate change. D J Carson
CRTN 10	Apr 1991	Use of wind stresses from operational N.W.P. models to force an O.G.C.M. of the Indian Ocean. D J Carrington
CRTN 11	Jun 1991	A new daily Central England Temperature series, 1772-1991. D E Parker, T P Legg and C K Folland
CRTN 12	Jul 1991	Causes and predictability of Sahel rainfall variability. D P Rowell, C K Folland, K Maskell, J A Owen, M N Ward

CLIMATE RESEARCH TECHNICAL NOTES

CRTN 13	Jul 1991	Modelling changes in climate due to enhanced CO2, the role of atmospheric dynamics, cloud and moisture. C A Senior, J F B Mitchell, H Le Treut and Z-X Li
CRTN 14	Sep 1991	Sea temperature bucket models used to correct historical SST data in the Meteorological Office. C K Folland
CRTN 15	Aug 1991	Modelling climate change, and some potential effects on agriculture in the U.K. P R Rowntree, B A Callander and J Cochrane
CRTN 16	Aug 1991	The Boreal Forests and Climate G Thomas and P R Rowntree
CRTN 17	Aug 1991	Development of a Stratosphere-Troposphere Data Assimilation System. R Swinbank.
CRTN 18	Sep 1991	A study of asynchronous coupling using a simple climate model. M K Davey.
CRTN 19	Sep 1991	The Oceanic Carbon Cycle. N K Taylor
CRTN 20	Nov 1991	Worldwide ocean-atmosphere surface fields in Sahel wet and dry years using provisionally corrected surface wind data. M N Ward
CRTN 21	Dec 1991	Coupled tropical ocean global atmosphere models at the UKMO. M K Davey, C Gordon, S Ineson and S Lawrence
CRTN 22	Dec 1991	Empirical parameterisation of tropical ocean-atmosphere coupling. M Allen, M K Davey, D L T Anderson and P D Killworth
CRTN 23	Feb 1992	The temporal evolution of Equatorial Currents in the Indian Ocean D L T Anderson, D J Carrington, R A Corry and C Gordon
CRTN 24	Feb 1992	Stratospheric analyses provided by the U.K. Meteorological Office M J Bailey, A O'Neill and V D Pope

CLIMATE RESEARCH TECHNICAL NOTES

CRTN 25	Feb 1992	Modelling interannual variability in the Indian Ocean using momentum fluxes from the UKMO and ECMWF operational weather analyses. D L T Anderson and D J Carrington
CRTN 26	Mar 1992	A GCM simulation of the impact of Amazonian deforestation on climate using an improved canopy representation J Lean and P R Rowntree
CRTN 27	Mar 1992	The parameterization of rainfall interception in GCMs A J Dolman and D Gregory
CRTN 28	Jun 1992	Development of worldwide marine data eigenvectors since 1985 A W Colman
CRTN 29	Jun 1992	A tropical ocean model with reduced physics M K Davey
CRTN 30	Jun 1992	International Temperature Workshop, Boulder, Colorado, USA, 16 January 1992 Edited by D E Parker
CRTN 31	Jul 1992	Simulation of clear-sky outgoing longwave radiation over the oceans using operational analyses A Slingo and M J Webb
CRTN 32	Sep 1992	A prediction of the transient response of climate J M Murphy
CRTN 33	Nov 1992	LEPS scores for assessing climate model simulations and long-range forecasts. C K Folland
CRTN 34	Jan 1993	Stratospheric Data Assimilation System Guide Editer: R Swinbank
CRTN 35	Mar 1993	A Stratosphere-Troposphere Data Assimilation System R Swinbank and A O'Neill
CRTN 36	Mar 1993	Validation of hydrological schemes for climate models against catchment data. P R Rowntree and J Lean

CLIMATE RESEARCH TECHNICAL NOTES

CRTN 37	Apr 1993	Modelling of palaeoclimates: Examples from the recent past J F B Mitchell
CRTN 38	May 1993	A simulation of seasonality in ENSO forecast skill M K Davey, D L T Anderson and S Lawrence
CRTN 39	Jul 1993	ENSO Prediction experiments using a simpe ocean-atmosphere model D-H Wu, D L T Anderson and M K Davey
CRTN 40	Sep 1993	Diagnosis of dynamic sea-surface and sea-level changes from the Cox ocean model J M Gregory
CRTN 41	Sep 1993	Seasonal variations of the clear-sky greenhouse effect: the role of changes in atmospheric temperatures and humidities M J Webb, A Slingo and G L Stephens